Fibers and Polymers (2024) 25:4831–4844
https://doi.org/10.1007/s12221-024-00742-x

Online ISSN 1875-0052
Print ISSN 1229-9197

REGULAR ARTICLE

An Experimental Investigation on Dynamic Behaviors of Shear Thickening Fluid Impregnated Aramid Fabrics for Different Number of Layers

Ali İmran Ayten[1,2] · **Alper Kaşgöz**[1]

Received: 31 May 2024 / Revised: 25 September 2024 / Accepted: 4 October 2024 / Published online: 14 October 2024

Abstract
Shear thickening fluid (STF) is a solution performs an increase in its viscosity under shear stress. This study investigates rheological behavior of STF, then its effectiveness against dynamic loadings for the case it is applied on aramid fabric. Polyethylene glycol 200 and 400 g/mol, and Aerosil 200, 300, 380 were used for preparation of STF. Rheological analysis was performed to determine thickening behavior and parameters for the solutions having 5, 10 and 20% silica concentrations by weight. The solution having optimum shear thickening performance for dynamic impact loading was selected and it was impregnated aramid fabric to prepare low velocity impact and ballistic test samples. Low velocity impact experiments were executed for different number of layers from 1 to 8 at different energy levels to obtain absorbed energy and maximum contact force values. A curve fitting equation was derived for absorbed energy and number of layers of aramid fabric. Finally, Level IIA ballistic test was done to test whether the curve fitting equation is effectively working or not. Additionally, STF impregnated aramid fabric with its neat counterpart against ballistic impact was compared. A detailed ballistic test characterization was performed including the last shape of ammo. It is determined that impregnation of STF has important effects on ballistic behavior of aramid fabric.

Keywords Aramid fabric · Shear thickening fluid · Rheology · Low velocity impact · Ballistic impact

1 Introduction

Increasing energy absorption capability of structures is one of the most important aims for researchers. Providing this purpose can be achieved through several methods such as modifying materials [1, 2], optimizing geometry [3–5] or designing hybrid structure [6, 7]. Applying shear thickening fluid (STF) onto fibers is the most common way to increase energy absorption of soft structures, especially in low velocity impact [8–10], high strain rate impact [11–16] and ballistic impact applications [17–25]. STF is a solution containing at least two components which one of them is carrying fluid and the other one is nanoparticles which is the providing "thickening" behavior of the solution. Nanoparticles shows agglomeration when shear loading was applied onto the structure. Presence of a carrier fluid such as polyethylene glycol on aramid fabric surface allows to move nanoparticles and their agglomeration due to their high surface area and van der Waals force. Physical properties of components comprised to STF have critical importance on the energy absorption behavior of structure due to the difference in final rheological behavior of STF. Different fillers can also be added into the structure of STF such as silicon carbide, aluminum oxide, boron carbide. Gürgen et al.[26] investigated the effect of these three types of additive particles on the behavior of PEG based STF colloidal solution. They prepared mixtures including 5%, 25% and 45% additives by weight and investigated the rheological behavior of STF. Higher concentration of additives presented higher thickening ratio and critical shear rate. In sum, it is concluded that STF included fillers might be useful in engineering applications where higher viscosity and lower thickening ratio needed. Khodadadi et al.[21] formulated shear thickening fluids (STFs) incorporating silica nanoparticles at

✉ Ali İmran Ayten
aiayten@yalova.edu.tr

[1] Faculty of Engineering, Department of Polymer Materials Engineering, Yalova University, 77200 Yalova, Turkey

[2] Faculty of Engineering, Department of Mechanical Engineering, Yalova University, 77200 Yalova, Turkey

varying weight percentages as 15%, 25%, 35%, and 45%. Their investigation focused on assessing the energy dissipation characteristics of these formulations. Through ballistic testing, they noted an enhancement in energy dissipation for fabrics treated with STFs; however, formulations with higher concentrations of nanosilica displayed an adverse effect. Their analysis revealed that the specific energy dissipation of Kevlar fabric treated with 15% filler STFs was inferior to that of untreated Kevlar fabric. Conversely, Kevlar fabric treated with 35% filler STFs exhibited a specific energy dissipation value 2.3 times greater than that of neat counterpart. STF is not only used in soft structures but has also been used in different material combinations including fabric such as sandwich structures. Zhang et al.[27] studied to enhance fabric stab resistance, needle-punching processing technology is employed to combine aramid fabric and nonwoven fabric. Shear thickening fluid (STF) and thermoplastic polyurethanes (TPU) were utilized to manufacture stab-resistant sandwich structures in various configurations. The stab resistance, bursting performance, and flexibility of these composites were discussed. Findings reveal that stab-resistant composites infused only STF and those with STF combined with TPU coating exhibit significant enhancement in stab resistance performance with minimal reduction in flexibility. During puncture, the shear thickening effect of STF accompanies the process, while the stab-resistant composite impregnated with STF and coated with TPU manifests a more cohesive fiber bonding.

Impregnated STF into the aramid fabric can increase areal weight of fabric at an acceptable ratio in exchange for a reduction of back face deflection of aramid fabric against ballistic threat. Bajya et al.[24] investigated various design strategies for soft armor panels utilizing shear thickening fluid (STF)-reinforced Kevlar fabric. Two types of STFs, having diameters of 500 nm and 100 nm, respectively, in polyethylene glycol (PEG) 200 were studied. STF impregnation of Kevlar fabrics is shown to reduce back face deflection (BFD) by 2.5 mm–2.8 mm while maintaining the same areal density of the panel (5 kg/m^2). By strategically placing STF-impregnated fabrics at the rear side and neat fabrics at the strike face of the panel, the areal density of the soft armor panel can be further reduced by 10% (to 4.5 kg/m^2) while ensuring that BFD remains comparable to or lower than that of an STF-impregnated homogeneous panel. Furthermore, STF-impregnated panels are observed to stop the impacting bullet earlier than neat panels.

This study builds upon the findings of a previous work [28], where the low-velocity impact resistance of shear thickening fluid (STF)-impregnated aramid fabrics was investigated. In this work, a more comprehensive approach is adopted, expanding the focus to include ballistic performance in addition to low-velocity impacts. While both studies examine the effects of STF on aramid fabrics, this

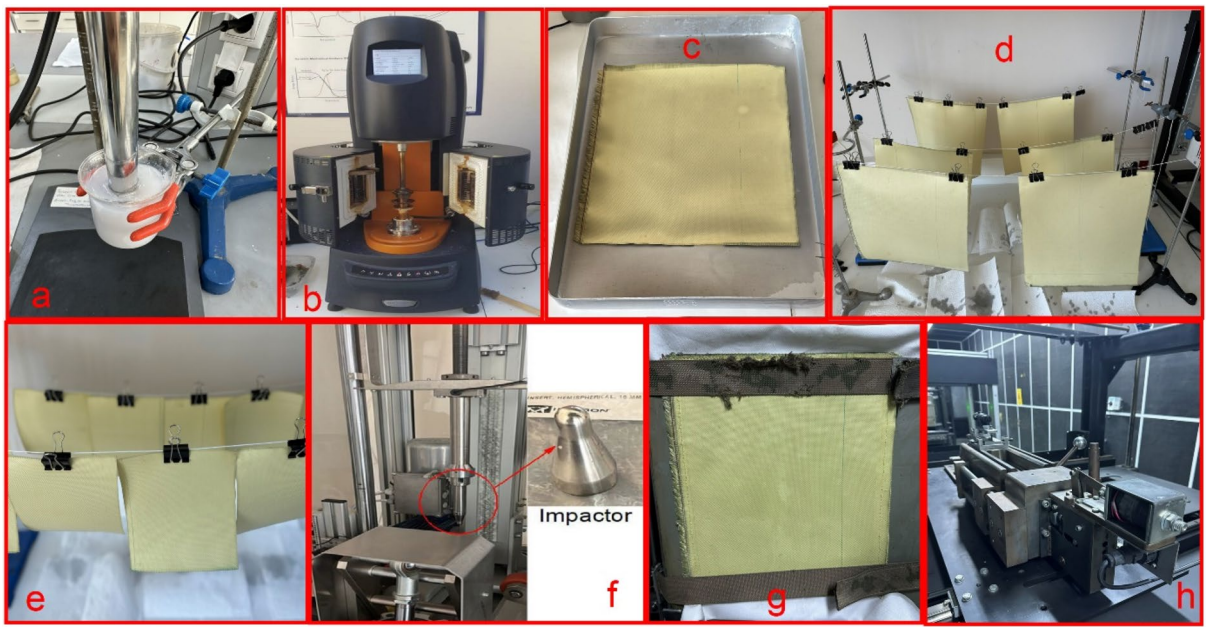

Fig. 1 All steps of methodology. **a** Preparation of shear thickening fluid, **b** rheological measurements of STF, **c** impregnation of STF into the aramid fabric, **d** hanging the large-scale fabric to a rope for drying, **e** drying small scale fabric, **f** low velocity impact experiment setup, **g** replacement of fabric for ballistic test, **h** ballistic test setup

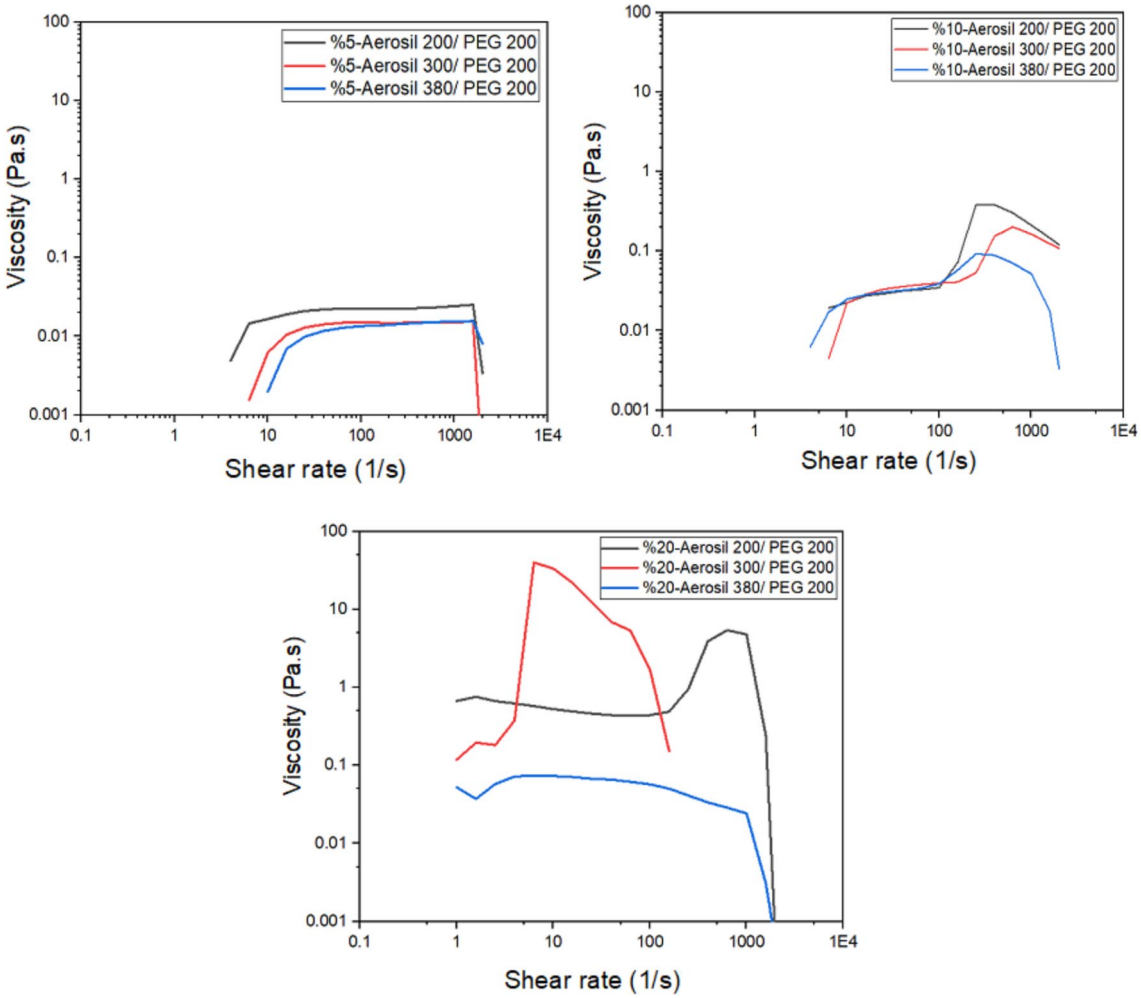

Fig. 2 Viscosity-shear rate graphs of solutions containing different sizes of silica nanoparticles and PEG 200 carrier fluid

paper provides a more detailed rheological analysis by incorporating different polyethylene glycol (PEG) carrier fluids (PEG200 and PEG400) and a wider variety of Aerosil nanoparticles (Aerosil 200, 300, 380). These analyses offer deeper insights into the impact of nanoparticle surface area and PEG type on the rheological properties of STF and its shear thickening behavior.

Additionally, this study introduces ballistic testing performed in accordance with the NIJ 0101.06 standard, offering a detailed evaluation of bullet deformation, damage area, and kinetic energy. This is a significant extension of the previous work, which focused solely on low-velocity impact tests. Furthermore, the relationships between damage dimensions, energy absorption capabilities, and the number of fabric layers are explored more extensively in this paper, using mathematical models to support the findings. Overall, this study provides a broader and more in-depth analysis, enhancing the potential applications and understanding of STF-impregnated fabrics in ballistic protection systems.

2 Materials and Method

Two different polyethylene glycol (PEG) PEG200 and PEG400 chemicals were used as distribution media while three different hydrophobic fumed silica nanoparticles Aerosil 200, 300 and 380 (Evonik Ltd.) were used for dispersion in polymer media. Solutions were prepared 5, 10, 20% containing silica nanoparticles by weight. Figure 1 summarizes

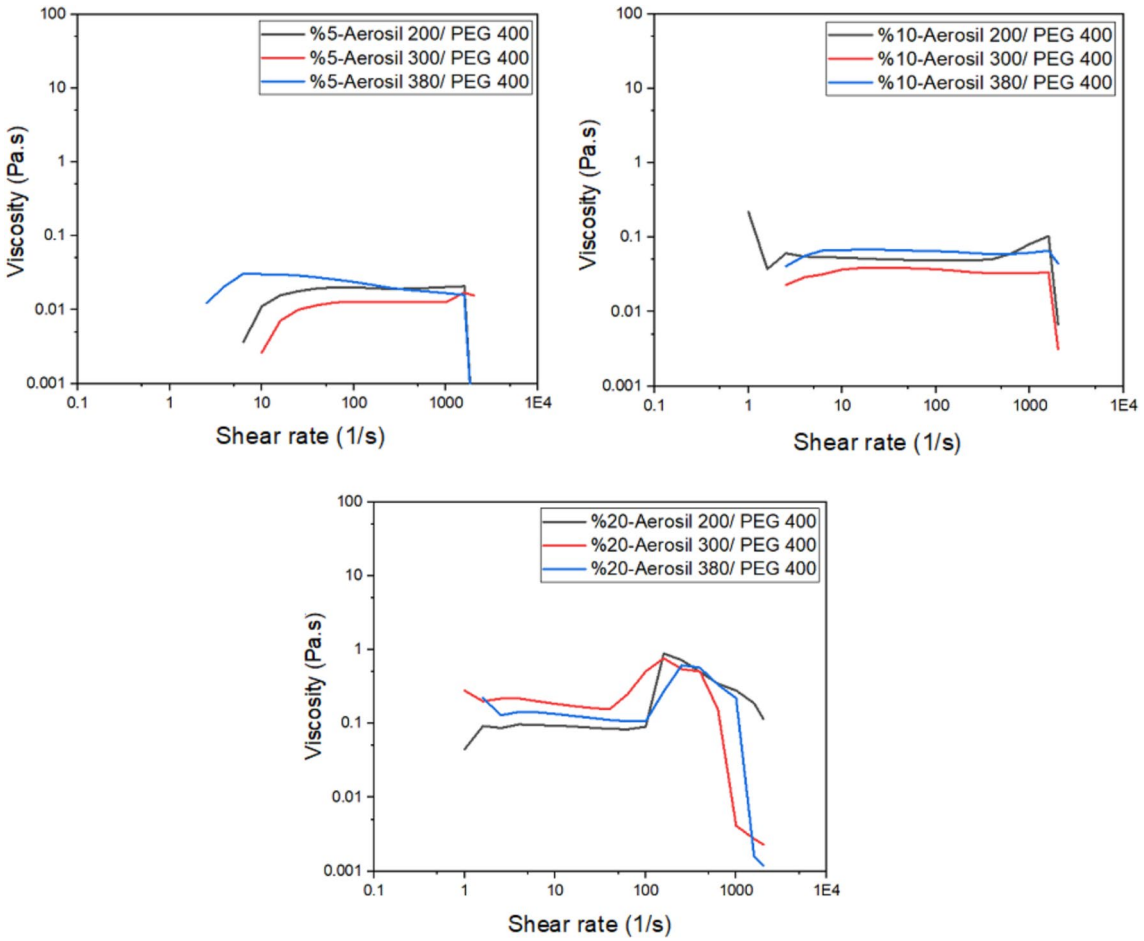

Fig. 3 Viscosity-shear rate graphs of solutions containing different sizes of silica nanoparticles and PEG 400 carrier fluid

all steps from preparation of STF to ballistic test of STF impregnated fabric. First, PEG and ethanol were mixed by a homogenizer (IKA T18 Basic Ultra Turrax) for 15 min at 3000–3500 rpm (Fig. 1a). Solution was waited at room temperature for 1 day to remove air bubbles its inside. Rheology analysis was performed by a rotational dynamic oscillatory hybrid rheometer (TA Instruments, Discovery HR-1) with 25 mm diameter parallel plates within a shear strain rate of 1 to 2250 s^{-1} at room temperature (Fig. 1b). STF solution was impregnated to both small scale specimen for low velocity impact test and large-scale specimen for ballistic impact test in an aluminum container then they attached to a rope to remove excess amount of the ethanol and solution (Fig. 1c-d-e). Twaron CT709 belongs to Teijin Ltd. aramid fabric has areal weight of 200 g/m^2 was used in all stages of this study. To understand the response of fabric specimens against low energy levels, low velocity impact test was performed at different amount of energy varying from 20 to 240 J by using Instron Ceast 9350 drop tower impact system (Fig. 1f).

Then, large scale fabric specimens were subjected to ballistic impact by a 9×19 mm parabellum lead core bullet which is IIA level ammunition specified in the NIJ 0101.06 standard (Fig. 1g-h). The mass of the bullet as specified in the standard is 8 g and its velocity is 373 m/s ± 9.1 m/s. Three samples were tested as 16 layers neat, 16 layers STF impregnated and 24 layers STF impregnated. The specimens were fixed on a conditioned clay at a certain temperature to determine the depth of penetration. Test setup includes two velocity sensors, as can be seen in Fig. 1h. Each sensor collects two measurements at inlet and outlet, and the average

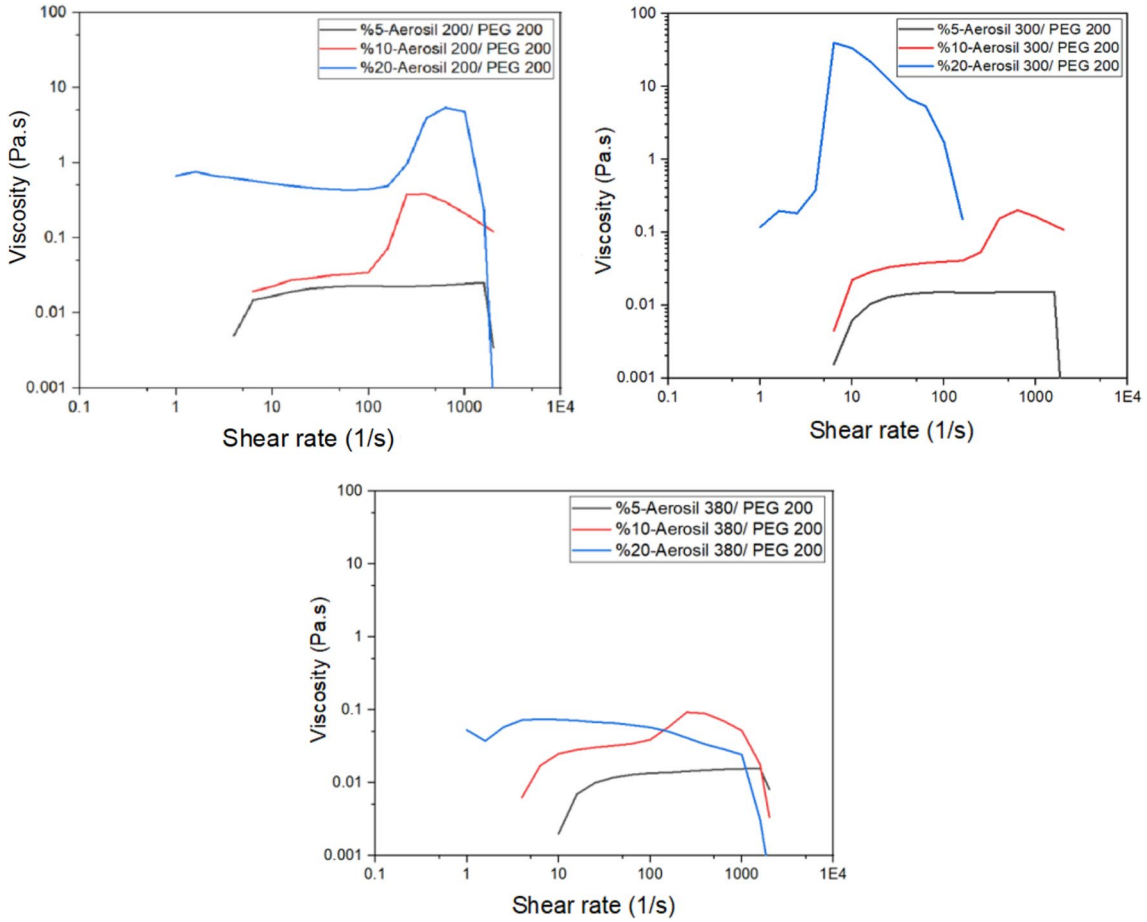

Fig. 4 Comparison of silica nanoparticle concentration for STF solutions with PEG 200 as the carrier phase

of these velocities appears as V_{12} on the first sensor and V_{34} on the second sensor. The average of V_{12} and V_{34} speeds is considered the velocity of that test and kinetic energy is calculated accordingly. After the experiments completed, the perforation/penetration conditions were examined, on the other hand, the damage dimensions/types were interpreted for STF impregnated specimens and the reference sample.

3 Results and Discussions

3.1 Rheological Characterization

Figures 2–6 show the rheology analysis results of solutions containing 5, 10 and 20% Aerosil 200 (12 nm particle diameter), Aerosil 300 (7 nm particle diameter) and Aerosil 380 (7 nm particle diameter). Aerosil 300 and 380 products were chosen because they have different surface areas even though their particle diameters are the same. PEG 200 and PEG 400 were used as carrier fluid.

Figure 2 and 3 compares the silica nanoparticles types between themselves when silica concentration is kept constant. 5% concentration solutions have not shown any thickening behavior in both PEG 200 and PEG 400 carrier fluid. For 10% concentration solutions, it is clear that Aerosil 200/PEG 200 combination has performed the best thickening behavior. PEG400 including solutions did not perform any thickening behavior for 10% silica concentrations. Aerosil 300/PEG200 solution exhibited the highest thickening behavior among all solutions having 20% silica nanoparticles, but its critical shear rate value is so small that this is a drawback for high velocity impact applications.

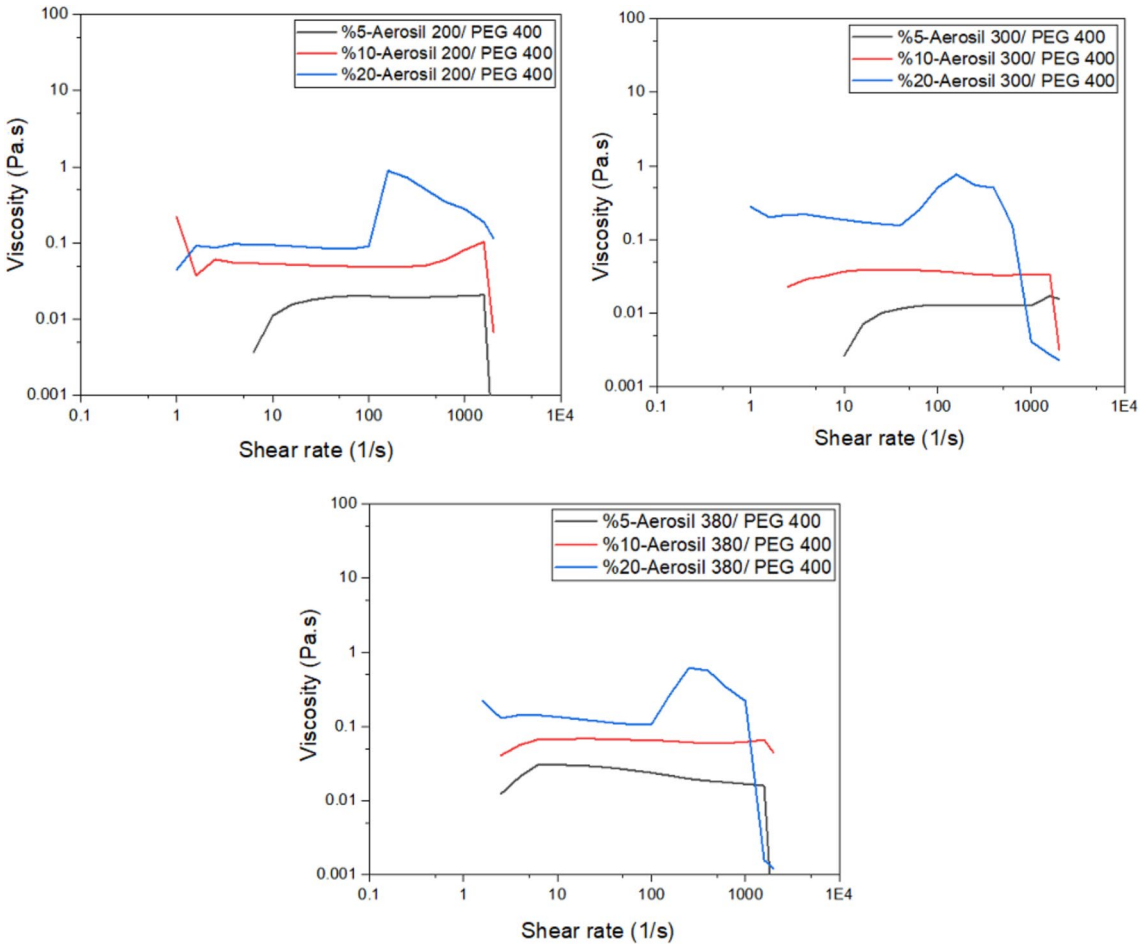

Fig. 5 Comparison of silica nanoparticle concentration for STF solutions with PEG 400 as the carrier phase

Figure 4 and 5 put the relationship between silica concentrations for the same type of Aerosil product. It can be seen that 20% silica concentration solutions performed the highest viscosity values. At lower silica concentrations, the suspension typically exhibits low viscosity and behaves like a Newtonian fluid or may show slight shear thinning. The onset of shear thickening occurs at higher shear rates because the particle spacing is relatively large, leading to weak hydrodynamic interactions. As the silica concentration increases, the distance between particles decreases. This causes to enhancing particle–particle interactions and shifting the onset of shear thickening to lower shear rates due to the simplification of hydrodynamic clustering and frictional contacts. Consequently, the increase in viscosity during shear thickening is more pronounced at higher concentrations because more particles interact to form stress-bearing structures under shear. Additionally, shear thickening behavior can shift from continuous to discontinuous with higher silica concentrations, characterized by an abrupt jump in viscosity at a critical shear rate due to sudden particle clustering.

Figure 6 compares two different carrier fluids for various silica nanoparticles which 20% concentrations, the most ideal one in terms of thickening behavior. The carrier fluid PEG200 exhibited higher maximum viscosity values and thickening behavior compared to PEG400 for Aerosil

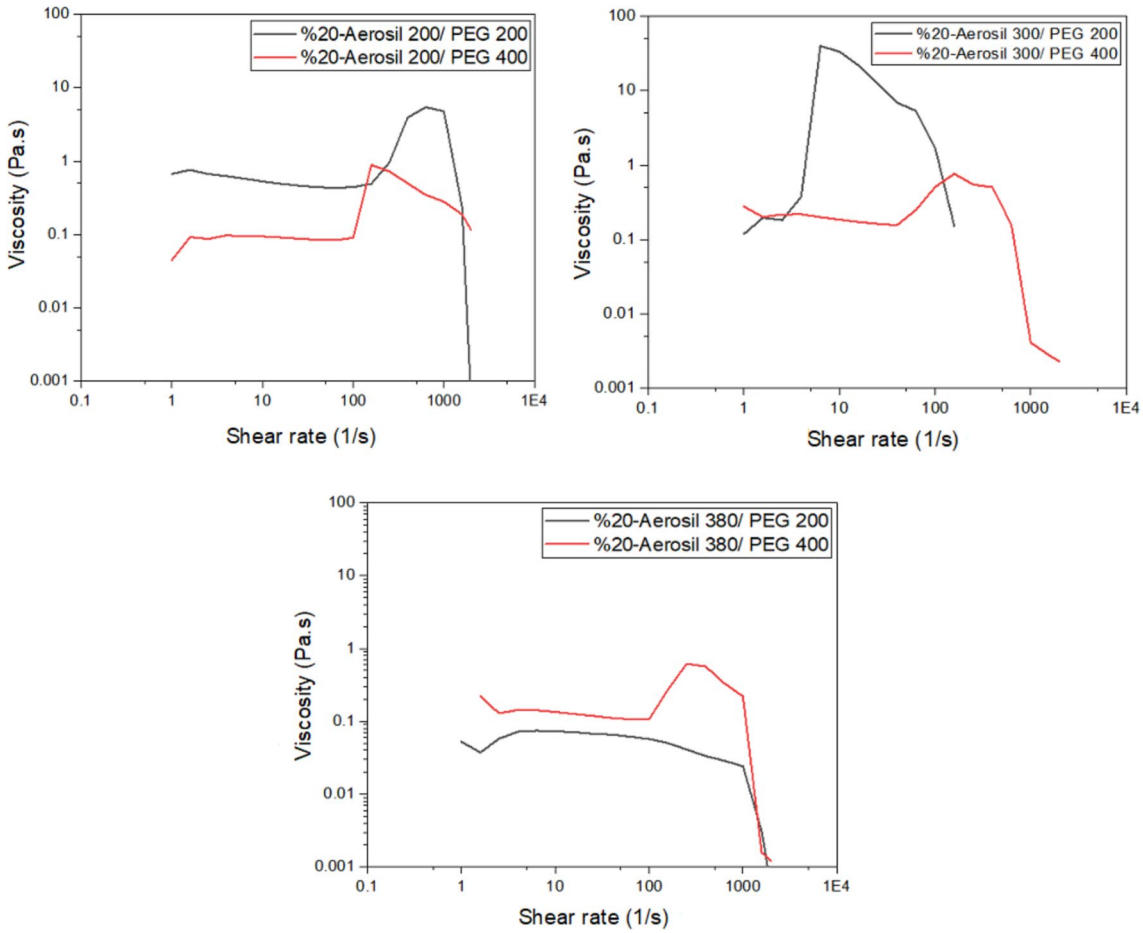

Fig. 6 Comparison of 20% silica nanoparticles STF solutions having different carrier phases and different diameter silica nanoparticles

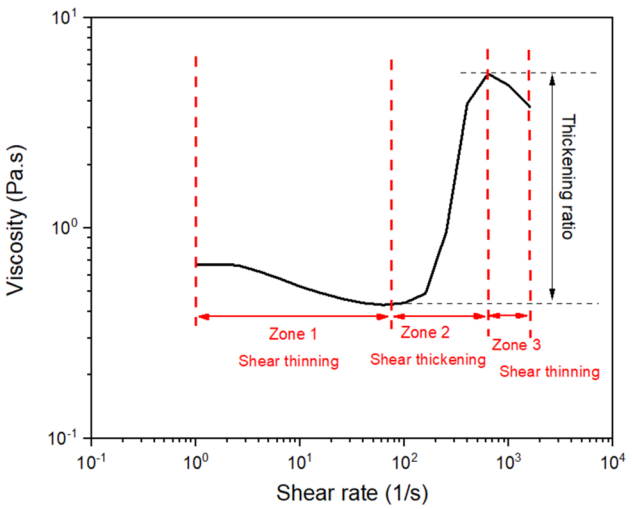

Fig. 7 Viscosity-shear rate relationship and thinning-thickening regions for Aerosil 200/PEG 200 STF solution [28]

200 and Aerosil 300 nanoparticles. However, this trend was reversed for Aerosil 380. When comparing candidates showing the best values to select the most ideal solution in the final stage, the solutions of Aerosil 200/PEG200 and Aerosil 300/PEG200 stand out. However, due to its thickening behavior not being desirable for ballistic applications, Aerosil 300/PEG200 was not preferred as it showed thickening at low values such as a shear rate of 10/s. When comparing Aerosil 200/PEG200 and Aerosil 380/PEG400 solutions, it can be seen that thickening behaviors start at similar shear rates. However, Aerosil 200/PEG200 exhibited approximately 10 times higher maximum viscosity value compared to the other solution. Therefore, when evaluating the behaviors of all solutions, it was decided that the optimum behavior was exhibited by the mixture containing 20% silica nanoparticles, Aerosil 200/PEG200.

Figure 7 shows the stages of viscosity change for Aerosil 200/PEG 200 STF solution. Herein, specimen performs shear thinning up to critical shear rate value. Then, agglomeration starts when thinning ended. Subsequently,

Table 1 Rheological characterization results of shear thickening fluids

Solution	Critical viscosity [Pa.s]	Critical shear rate [s^{-1}]	Peak viscosity [Pa.s]	Shear rate at maximum viscosity [s^{-1}]	Thickening ratio (times)
%5 Aerosil 200/PEG200	0.015	6.4	0.0253	1580	**1.687**
%5 Aerosil 200/PEG400	0.011	10	0.020	1584	**1.818**
%5 Aerosil 300/PEG200	0.0062	10	0.0153	1585	**2.468**
%5 Aerosil 300/PEG400	0.007	15.85	0.017	1584	**2.429**
%5 Aerosil 380/PEG200	0.007	15.85	0.0156	1585	**2.229**
%5 Aerosil 380/PEG400	0.03	6.3	0.0159	1585	**0.53**
%10 Aerosil 200/PEG200	0.0347	100	0.38	251	**10.95**
%10 Aerosil 200/PEG400	0.061	2.51	0.1038	1585	**1.70**
%10 Aerosil 300/PEG200	0.0268	39.8	0.041	1000	**1.53**
%10 Aerosil 300/PEG400	0.0387	15.85	0.0333	1585	**0.86**
%10 Aerosil 380/PEG200	0.0248	10	0.0923	251	**3.72**
%10 Aerosil 380/PEG400	0.0674	10	0.066	1585	**0.979**
%20 Aerosil 200/PEG200	0.43	63	5.42	631	**12.6**
%20 Aerosil 200/PEG400	0.083	63	0.884	158.5	**10.65**
%20 Aerosil 300/PEG200	0.182	2.51	39.75	6.31	**218.4**
%20 Aerosil 300/PEG400	0.155	39.8	0.764	158.48	**4.93**
%20 Aerosil 380/PEG200	0.0372	1.58	0.0744	6.31	**2**
%20 Aerosil 380/PEG400	0.107	100	0.615	251.2	**5.748**

Bold numbers are indicate the most critical results

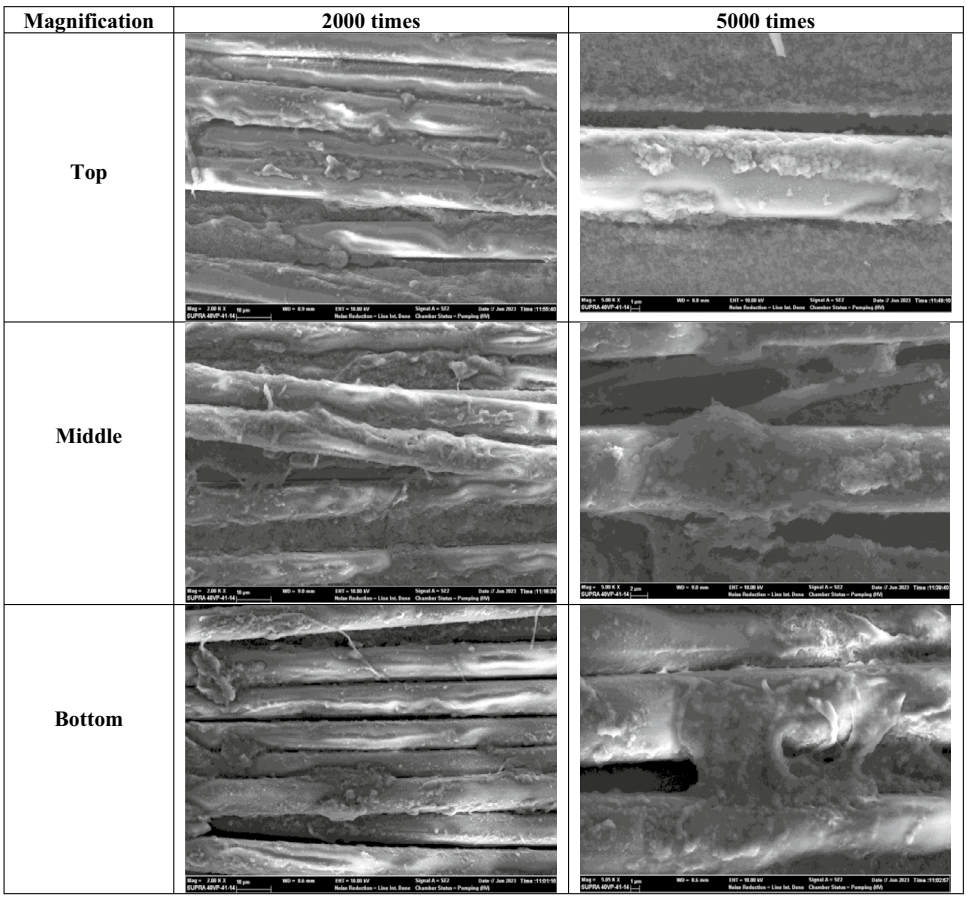

Fig. 8 SEM images at different magnifications captured from different regions of the STF impregnated fabric after drying

Table 2 Top and bottom views of STF impregnated aramid fabrics after low velocity impact test.

Number of layers	Top view	Bottom view	Damaged area (cm^2)
1	 I.E.= 20 J; A.E.= 16.3 J		48.4
2	 I.E.= 30 J; A.E.= 24 J		67.3
3	 I.E.= 40 J; A.E.= 40 J		73.4
4	 I.E.= 70 J; A.E.= 70 J		99

Table 2 (continued)

5	 I.E.= 90 J; A.E.= 90 J		**108.4**
6	 I.E.=120 J; A.E.= 115 J		**111.3**
7	 I.E.= 180 J; A.E.= 150 J		**128.4**
8	 I.E.= 240 J.; A.E.= 180 J.		**137.3**

I.E Impact Energy, *A.E* Absorbed energy.

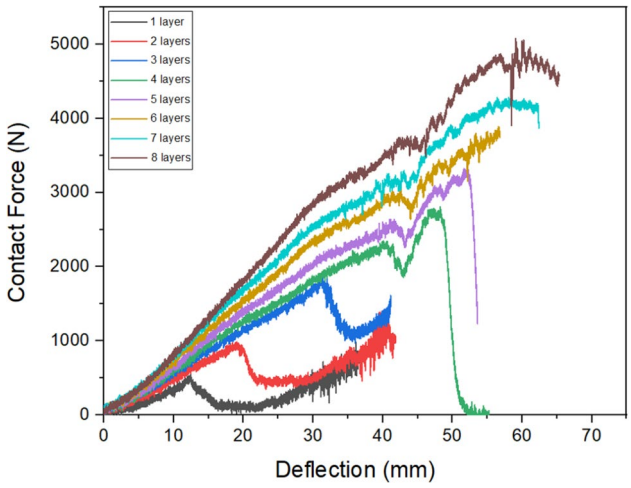

Fig. 9 Contact force–deflection curves for different number of layers STF (Aerosil 200/PEG200) impregnated fabric specimens [28]

shear thickening continues up to maximum viscosity value then another thinning behavior can be observed for a short time.

Table 1 presents a brief summary of the Figs. 2, 3, 4, 5, 6 in terms of shear thickening behavior parameters such as critical viscosity, critical shear rate, peak viscosity, and thickening ratio (peak viscosity/critical viscosity). In this table, Aerosil 300/PEG200 solution having 20% concentration performed the highest thickening ratio but as it was mentioned above, critical shear rate value of this solution is so small when it compares to Aerosil 200/PEG200 solution. This was the main reason why 20% concentrate Aerosil 200/PEG 200 solution was selected for impact applications.

3.2 SEM analysis

After the aramid fabric was impregnated with STF, it was dried by hanging to a rope for 24 h to remove the ethanol from its structure. Because the fabric was exposed to the gravity during this period, SEM samples were taken and examined from the upper, middle, and lower regions of a reference sample to ensure that the PEG/nanosilica mixture properly adhered to the structure. Figure 8 shows the images from the upper, middle, and lower regions at 2000 × and 5000 × magnifications. As can be seen from the figure, the mixture adheres to the fiber structure and displays a similar appearance at 2000 times magnification. Therefore, drying was continued with this method throughout this study.

3.3 Low Velocity Impact Test Results

Table 2 presents top and bottom views of damaged samples at the end of low velocity impact tests from 1 to 8 layers of STF impregnated fabric. Equation (1) put a relationship

Table 3 Absorbed energy and maximum contact force values depend on the number of fabric layers

Number of layers	1	2	3	4	5	6	7	8
Absorbed Energy (J)	16.3	24	40	70	90	115	150	180
Maximum Contact Force (N)	487	935	1748	2716	3278	3852	4230	4888

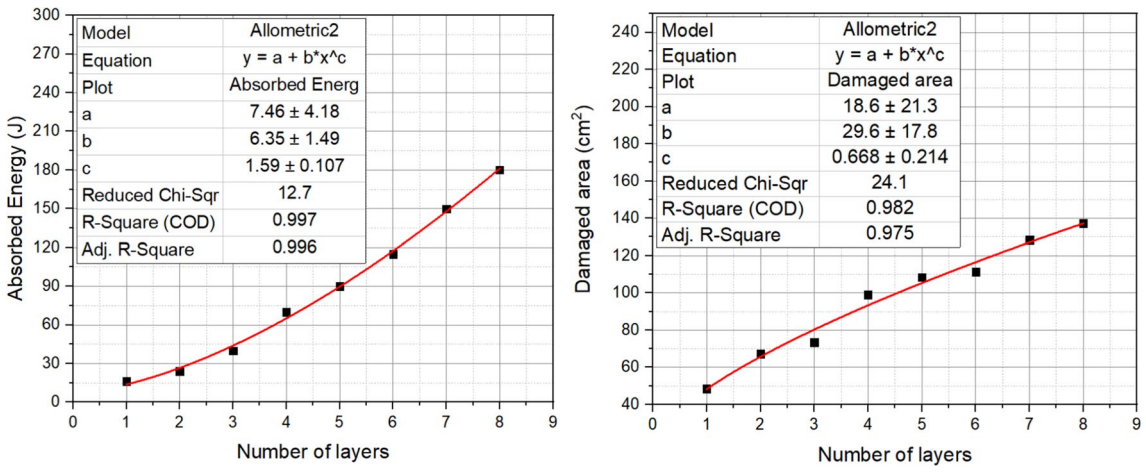

Fig. 10 Absorbed energy and number of layers relationship (left). Curve fitting equation to describe the relationship between damaged area and number of layers (right)

Table 4 Front and back views of large-scale aramid fabric specimens used in ballistic experiments.

	Front	Back
16 layers neat fabric	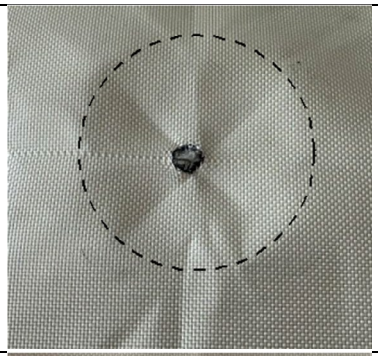	
16 layers STF impregnated fabric	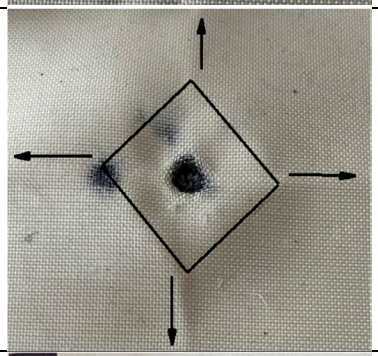	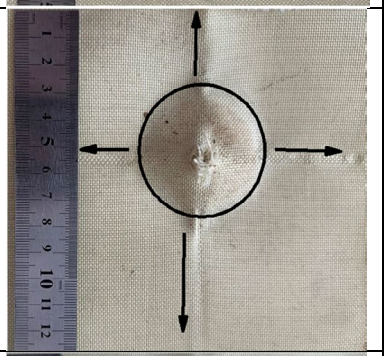
24 layers STF impregnated	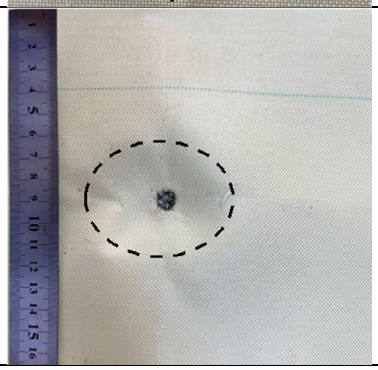	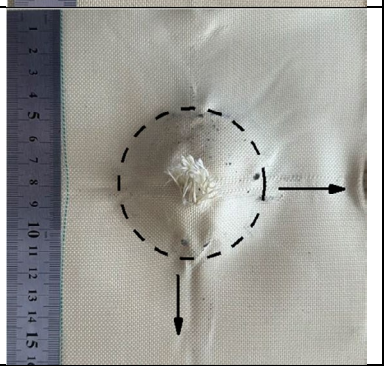

between absorbed energy and number of layers while Eq. (2) presents a relationship between damage area and number of layers. Damage area of fabric is getting increase with the increasing number of layers.

Figure 9 shows force–displacement curves corresponding to aramid fabric specimen ranging from 1 to 8 layers. The curves include noise due to contact issues between the impactor and the soft form fabric. Examination of the initial 10 mm displacement reveals a proportional increase in stiffness with the increasing number of fabric layers. Notably, a clear 'V' shape appears in most of the curves around a 42 mm displacement, likely reflecting damage patterns as detailed in Table 2. The reason of initial load drop is the compaction of fabrics, leading to a subsequent rise in contact force. Energy absorption by the fabric specimens is calculated by integrating the area under the force–displacement curve, as per Eq. 1, where 'F' and 'δ' represents contact force and displacement, respectively. The resultant values are presented in Table 3 and plotted in Fig. 10 for curve fitting. The ratio of contact force between 1-layer and 2-layer specimens is 1.92, decreasing to 1.16 for 7-layer and 8-layer specimens. This observation suggests that beyond a certain layer count, specimen rigidity experiences a plateau effect.

$$y = 7.46 + 6.35(x^{1.59}) \tag{1}$$

$$y = 18.6 + 29.6(x^{0.668}) \tag{2}$$

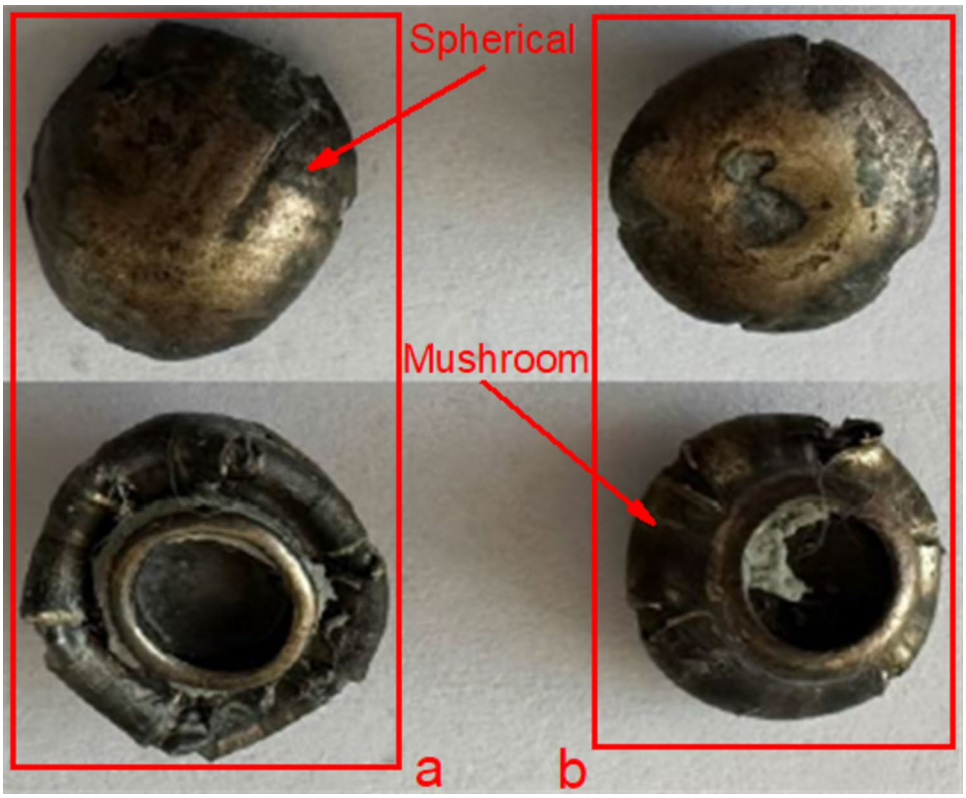

Fig. 11 End-of-test conditions of 9 mm bullets after ballistics tests for 16 layers of fabric. Bullet was fired against **a** STF impregnated fabric, and **b** neat fabric

Table 5 Velocities of bullets and their kinetic energies

	V_{12} (m/s)	V_{34} (m/s)	V_{mean} (m/s)	Kinetic Energy (J)	Damaged area on the back face (cm^2)
First shot (16 layers neat)	376.02	382.82	379.42	575.84	16
Second shot (16 layers STF impregnated)	399.55	406.21	402.88	649.25	18.5
Third shot (24 layers STF impregnated)	392.05	399.65	395.85	626.79	37

3.4 Ballistic Test Results

More bulky back-face damage area was observed in STF-impregnated fabric specimens as shown in Table 4. PEG chemical in shear thickening fluid provides a sticky surface to aramid fabric and this helps to hold fabric layers together which contributes to increasing the rigidity of structure.

Final conditions of 9 mm bullets can be seen in Fig. 11. There is a clear difference between bullets in terms of their final shapes and deformation patterns. Top of final shape of the bullet was fired against STF-impregnated fabric specimen was spherical while the top of the other bullet was mushroom shape. The first bullet (Fig. 11a) was deformed as getting folded inside while the other one is deformed a certain level. This difference may be explained by STF impregnated fabric applied higher reaction force to the bullet than its neat counterpart. Silica nanoparticles in carrier fluid getting agglomerated and cause more rigid behavior of fabric. This mechanism creates an extra reaction force onto the bullet, so it is getting folded its inside (Table 5).

4 Conclusions

This study focused on the rheological behavior of shear thickening fluids and the effects of STF on dynamic response of aramid fabric. Rheological test, low velocity impact test, and ballistic test were conducted to determine thickening parameters, energy absorption values for low velocity and ballistic impact. Aerosil 200/PEG 200 solution having 20% concentration showed 12.6 times thickening. Analytical equation was determined between absorbed

energy and number of layers from low velocity impact test results. STF impregnated sample had 16% more damage area than its neat counterpart. It means STF impregnated sample absorbed more kinetic energy at this rate. Also, damage pattern of bullet was completely different in STF impregnated sample due to its bulk structure.

Acknowledgements This work was supported by Yalova University Scientific Research Projects Unit (BAP) (Project No: 2020/AP/0013). The authors would like to express their thanks for funding. Also, the authors are grateful to Teijin Ltd. and Evonik Ltd. companies for their support in material supply.

Funding Yalova University Scientific Research Projects Unit,2020/AP/0013, Ali Imran Ayten

Data availability All data generated or analyzed during this study are included in this article.

Declarations

Conflict of interest We have no conflicts of interest to declare.

References

1. T. Hai, F. Mohammed Alhomayani, K. Sharma, J. Mol. Liquids (2023). https://doi.org/10.1016/j.molliq.2023.122592
2. V.A. Chatterjee, S.K. Verma, D. Bhattacharjee, I. Biswas, S. Neogi, Composite Struct (2019). https://doi.org/10.1016/j.compstruct.2019.111148
3. M.M. Awd Allah, W. Abdel-Aziem, M.A. Abd El-baky, Fibers and Polym. (2023). https://doi.org/10.1007/s12221-023-00207-7
4. N.N. Hussain, S.P. Regalla, Y.V.D. Rao, T. Dirgantara, L. Gunawan, A. Jusuf, Proceedings of the institution of mechanical engineers. J. Mater. Design and Appl. **235**, 114 (2020)
5. A. Ciampaglia, D. Fiumarella, C. Boursier Niutta, R. Ciardiello, G. Belingardi, Compost. Struct. (2021). https://doi.org/10.1016/j.compstruct.2020.113093
6. C. Caglayan, I. Osken, A. Ataalp, H.S. Turkmen, H. Cebeci, Comp. Struct. (2020). https://doi.org/10.1016/j.compstruct.2020.112171
7. K. Fu, H. Wang, L. Chang, M. Foley, K. Friedrich, L. Ye, Compos. Sci. Technol. **165**, 74 (2018)
8. J. Lim, S.-W. Kim, Compos. Struct. (2023). https://doi.org/10.1016/j.compstruct.2023.117349
9. H. Taş, I.F. Soykok, Fibers Polym. **22**, 2626 (2021)
10. U. Mawkhlieng, A. Majumdar, D. Bhattacharjee, Fibers and Polym. **22**, 213 (2021)
11. X. Zhang, P. Wang, A. Kurkin, Q. Chen, X. Gong, Z. Zhang, E.-H. Yang, J. Yang, Intern J Mech Sci (2021). https://doi.org/10.1016/j.ijmecsci.2021.106304
12. S. Laifa, D.E. Tria, M. Derradji, S. Khalfallah, Thin-Wall. Struct. (2023). https://doi.org/10.1016/j.tws.2023.111133
13. A. Laha, A. Majumdar, Mater. Des. **89**, 286 (2016)
14. K. Fu, H. Wang, S. Wang, L. Chang, L. Shen, L. Ye, Mater. Des. **140**, 295 (2018)
15. S. Cao, Q. Chen, Y. Wang, S. Xuan, W. Jiang, X. Gong, Compos. A Appl. Sci. Manuf. **100**, 161 (2017)
16. N. Asija, H. Chouhan, S.A. Gebremeskel, N. Bhatnagar, Int. J. Impact Eng **110**, 365 (2017)
17. S. Arora, A. Majumdar, B.S. Butola, Comp. Struct. (2020). https://doi.org/10.1016/j.compstruct.2019.111720
18. A.F. Ávila, A.M. de Oliveira, S.G. Leão, M.G. Martins, Compos. A Appl. Sci. Manuf. **112**, 468 (2018)
19. S. Gürgen, M.C. Kuşhan, Polym. Test. **64**, 296 (2017)
20. E.E. Haro, A.G. Odeshi, S. Castellanos, X. Sanchez, L. Abatta, L. Criollo, A. Alban, J.A. Szpunar, Comp. Open Access (2023). https://doi.org/10.1016/j.jcomc.2023.100420
21. A. Khodadadi, G. Liaghat, S. Vahid, A.R. Sabet, H. Hadavinia, Compos. B Eng. **162**, 643 (2019)
22. E.D. Lee, N.J. Wagner, J. Mater. Sci. (2003). https://doi.org/10.1023/A:1024424200221
23. V.D. Mishra, A. Mishra, A. Singh, L. Verma, G. Rajesh, Compos. Struct. (2022). https://doi.org/10.1016/j.compstruct.2021.114991
24. M. Bajya, A. Majumdar, B.S. Butola, S.K. Verma, D. Bhattacharjee, Compos. Eng. (2020). https://doi.org/10.1016/j.compositesb.2019.107721
25. Y. Zhang, L. Chang, J. Xu, T. Chen, Z. Mao, Z. Cai, Poly Compos. (2024). https://doi.org/10.1016/j.matdes.2016.05.055
26. S. Gürgen, W. Li, M.C. Kuşhan, Mater. Des. **104**, 312 (2016)
27. X. Zhang, T.-T. Li, H.-K. Peng, C.-W. Lou, J.-H. Lin, Compos. Struct. (2022). https://doi.org/10.1016/j.compstruct.2021.114930
28. A.İ Ayten, Bitlis Eren Üniversitesi Fen Bilimleri Dergisi **12**, 887 (2023)